Journal of Molecular Spectroscopy 278 (2012) 1–6

Contents lists available at SciVerse ScienceDirect

Journal of Molecular Spectroscopy

journal homepage: www.elsevier.com/locate/jms

# State purity of decelerated molecular beams

N.J. Fitch, D.A. Esteves, M.I. Fabrikant, T.C. Briles, Y. Shyur, L.P. Parazzoli, H.J. Lewandowski *

*JILA and Department of Physics, University of Colorado, 440 UCB, Boulder, CO 80309-0440, United States*

ARTICLE INFO

*Article history:*
Received 22 May 2012
In revised form 26 June 2012
Available online 20 July 2012

*Keywords:*
Stark deceleration
Molecular beams
Cold molecules

ABSTRACT

Cold, velocity-controlled molecular beams consisting of a single quantum state are a powerful tool for exploring molecular interactions. Here, we explore the state purity and resulting dynamics of a Stark-decelerated beam of ammonia molecules where numerous rotational states are initially populated. Under these circumstances, Stark deceleration is shown to be ineffective at producing a molecular beam consisting of a single quantum state. Therefore, quantum state purity must be carefully considered when using Stark decelerated beams and analogous techniques, particularly in collision experiments where contributions from all quantum states must be addressed.

© 2012 Elsevier Inc. All rights reserved.

## 1. Introduction

Studying gas-phase molecular interactions where the reactants are in a single internal quantum state and have well-controlled external motion is one of the main goals in physical chemistry. Investigating interactions on a state-by-state level would facilitate exploration of the role of quantum mechanics in molecular processes. In the simplest case, interactions between molecules in ground-states may be energetically forbidden but are possible among excited states. More generally, reaction barriers and orientation-dependent interactions can all depend heavily on the specific quantum states involved. Various molecular spectroscopy experiments could also benefit from a source of single quantum-state molecules [1].

In addition to control over the reactants' internal (electronic, rovibrational) degrees of freedom, many experiments require control over the external (translational) degrees of freedom. In particular, collision experiments involving molecular beams often require the ability to produce a molecular sample with a well defined mean forward velocity and narrow velocity width. For example, studies of scattering resonances require a tunable forward velocity, so that the collision energy can be varied over the resonance, as well as a narrow velocity distribution to provide high energy resolution [2–4].

Several methods have been developed to produce cold molecular samples. These methods include supersonic expansion [5], buffer-gas cooling [6,7], velocity selection [8], kinematic cooling [9], photoassociation [10,11], Feshbach resonances [12,13], and a variety of beam deceleration techniques. Beam deceleration methods generally consist of decelerating a molecular beam produced via supersonic expansion using optical [14], magnetic [15] or electric fields [16]. To date, such approaches have successfully decelerated a number of chemically interesting molecular species, including CO, $NH_3$, $ND_3$, OH, $SO_2$, NH, CaF, $O_2$, and benzene [16–21,15,22]. In addition to studying the dynamics of the deceleration process itself, many groups are now using these beams to study molecular interactions [2,23–28].

In a general sense, all molecular beam deceleration approaches use the interaction between a molecule and an applied external field to apply a force that opposes the longitudinal velocity. Typically, this interaction is quantum state dependent. Thus, the presence of multiple quantum states that can be decelerated requires knowledge of the deceleration dynamics and their effect on the final state distribution. Explorations of beam-deceleration selectivity (i.e. the ability to filter out all but a single quantum state) have appeared previously in the literature. One study focused on the deceleration of different isotopologues [17] while another involved different projections of the dipole moment of the OH molecule onto the electric field axis [29]. While previous work has briefly explored state selectivity of the deceleration process, an in-depth study has not been performed. In addition to the selectivity, the resulting beam dynamics are of interest and also remain largely unexplored. For collision experiments involving decelerated beams, a full understanding of the beam dynamics is crucial for correctly interpreting experimental results.

Here we present experimental measurements and supporting simulations of a Stark decelerated beam consisting of numerous weak-field-seeking rotational states. The purpose of this study is to precisely quantify the state selectivity of molecular decelerators and to explore the resulting beam dynamics when multiple quantum states are present. The principal method used for this investigation is the deceleration and detection of various rotational states of a single isotopologue of ammonia. Specifically, molecules in two

* Corresponding author.
*E-mail address:* lewandoh@colorado.edu (H.J. Lewandowski).

0022-2852/$ - see front matter © 2012 Elsevier Inc. All rights reserved.
http://dx.doi.org/10.1016/j.jms.2012.07.005

rotational states, which have different Stark shifts, are decelerated and state-selectively detected using decelerator timing sequences corresponding to a large range of Stark shift to mass ratios. These measurements are compared to the results of a series of three-dimensional Monte Carlo simulations. We find that the Stark deceleration process is not highly quantum-state selective, but does produce differences in the final velocity distributions of the various states.

## 2. Stark deceleration

The Stark deceleration process begins with a pulsed supersonic expansion, where the molecules of interest are seeded at a low concentration in a heavier buffer gas. The resulting molecular beam is internally cold. If the molecule has multiple low lying, energetically accessible excited rotational states, as is the case with ammonia, a significant portion of the population can end up in these excited states. For molecules such as OH, where the first excited rotational state is $\sim$80 cm$^{-1}$ above the ground state, only the ground state will be substantially populated and rotational excitations can usually be neglected. Though internally cold, such beams have a high forward velocity in the laboratory frame of many hundreds of meters per second, which can be reduced by Stark deceleration.

The Stark deceleration technique [16] relies on the interaction of an electric field with a molecule's electric dipole moment to reduce the high forward velocity a portion of the molecular beam. A series of high-voltage electrode pairs create periodic electric field maxima along the beam axis. Any molecule whose energy increases with increasing electric field (known as a weak-field-seeking state) will experience an acceleration opposing its motion. As these molecules propagate into the increasing electric field, longitudinal kinetic energy is converted into potential energy. If the molecules were allowed to continue past the local electric field maximum they would regain their lost kinetic energy. However, before they reach the field maximum, the electric field is switched off rapidly, reducing the forward velocity of the beam by a small amount. This process is repeated using successive electrode pairs to produce a molecular beam with the desired final velocity. Transverse guiding is also achieved because the molecules are attracted to the electric field minimum along the center of the decelerator. To guide equally in both transverse dimensions, successive electrode pairs are oriented orthogonally to one another.

The final velocity of the decelerated molecules is determined by the amount of energy removed per stage and the total number of stages. The amount of energy removed per stage can be described by the position of the so-called "synchronous molecule", which is at the same physical location relative to each electrode pair at the time the electric fields are switched off. This position is referred to as the phase angle, $\phi_0$, where $\phi_0 = 0^\circ$ corresponds to no energy being removed and $\phi_0 = 90^\circ$ corresponds to the maximum amount of energy being removed. Increasing the phase angle, and hence the amount of energy removed per stage, results in both lower final velocities and lower overall molecule numbers [30]. This is because the phase-space acceptance, the region of phase space that will be decelerated and transported to the end of the decelerator, decreases with increasing phase angles.

Molecules close to the synchronous molecule in phase space experience an average force toward its location. This force results in an effective time-averaged moving potential well [17]. The dynamics of molecular trajectories in this moving potential well have been thoroughly investigated in the case where the molecules have the same mass and Stark shift as that of the synchronous molecule [31]. In the present analysis, molecules with the same mass but different Stark shifts are experimentally investigated. This required a molecular beam with many initially populated weak-field-seeking states. The numerous low-lying rotational states of the ammonia molecule (Fig. 1) are ideal for this purpose because of their appreciable Boltzmann factors at our beam temperature (6–7 K).

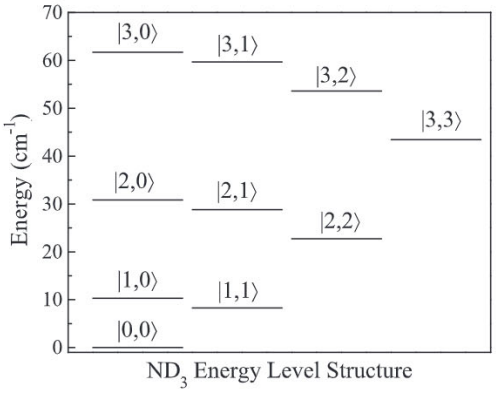


**Fig. 1.** Rotational energy levels of the ground electronic state in $^{14}ND_3$. The states are labeled by $|J,K\rangle$ and organized by $K$ value. The inversion splitting is not visible on this scale.

## 3. The ammonia molecule

In its rovibrational ground state, ammonia has a trigonal pyramidal structure with a ladder of rotational states denoted by $|J,K\rangle$, where $J$ is the total angular momentum and $K$ is the projection of $J$ onto the symmetry axis of the molecule. The trigonal pyramidal structure has two inversion eigenstates, which are symmetric and antisymmetric combinations of the two polarized "umbrella" states. The umbrella states are defined by the nitrogen being either "above" or "below" the plane defined by the hydrogen atoms. Because there is a barrier for the nitrogen to tunnel through this plane, the two eigenstates are separated in energy by an inversion splitting, $\Delta U_{inv}$, which varies only slightly among low rotational states (Table 1). When an electric field is applied, the two opposite-parity inversion states mix and are repelled from one another in energy. This Stark energy is given by

$$U_{stark} = \pm\sqrt{\left(\frac{\Delta U_{inv}}{2}\right)^2 + \left(|\vec{\mu}|\left|\vec{E}\right|\frac{MK}{J(J+1)}\right)^2} \mp \frac{\Delta U_{inv}}{2}, \quad (1)$$

where $\vec{\mu}$ is the electric dipole moment ($\mu_{ND_3} = 1.47$ Debye), $\vec{E}$ is the electric field, $M$ is the projection of $J$ onto the electric-field axis, and the upper (lower) signs correspond to weak- (strong-) field-seeking molecular states. Fully deuterated ammonia ($ND_3$) was chosen over $NH_3$ because of its favorable Stark shift due to its much smaller inversion splitting ($\sim$0.05 cm$^{-1}$ compared to $\sim$0.79 cm$^{-1}$ for $NH_3$).

## 4. Experiment

The experimental apparatus consists of a pulsed valve, Stark decelerator, and molecular detector comprised of a pulsed dye la-

**Table 1**
The energies, inversion splittings, and relative dipole moments for various rotational levels. Entries in the fourth column include all possible non-zero values of $M$.

| $\|J,K\rangle$ | $E_{rot}$ (cm$^{-1}$) | $\Delta U_{inv}$ (cm$^{-1}$) [32] | $\left\|\frac{\mu_{dl}}{\mu}\right\|$ |
|---|---|---|---|
| 1 1 | 8.26 | 0.0530 | 1/2 |
| 2 2 | 22.74 | 0.0525 | 2/3, 1/3 |
| 2 1 | 28.82 | 0.0520 | 1/3, 1/6 |
| 3 3 | 43.51 | 0.0518 | 3/4, 1/2, 1/4 |
| 3 1 | 53.60 | 0.0511 | 1/4, 1/6, 1/12 |
| 3 2 | 59.69 | 0.0506 | 1/2, 1/3, 1/6 |

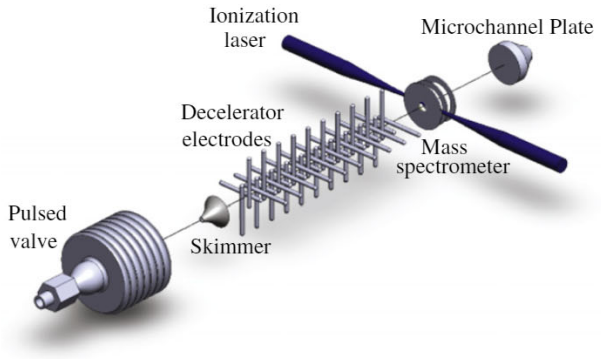


**Fig. 2.** Experimental set-up consisting of a PZT-driven pulsed valve, molecular beam skimmer, decelerator, time-of-flight mass spectrometer, and microchannel-plate ion detector. The decelerator consists of 150 electrode pairs (not all are shown).

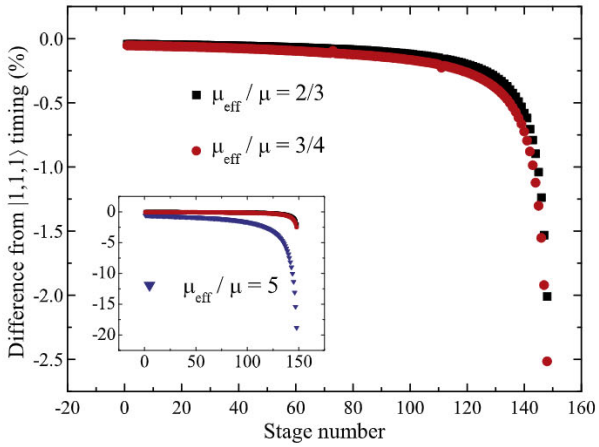


**Fig. 3.** Percent differences for the $\frac{\mu_{eff}}{\mu}=\frac{2}{3}$ ($|2,2,2\rangle$, squares) and the $\frac{3}{4}$($|3,3,3\rangle$, circles) timing sequences from the $\frac{\mu_{eff}}{\mu}=\frac{1}{2}$($|1,1,1\rangle$) for decelerating to 60 m/s. Inset: timing difference of the $\frac{\mu_{eff}}{\mu}=5$.

ser, time-of-flight mass spectrometer (TOFMS) and microchannel plate (MCP) (Fig. 2). A molecular beam is created by supersonic expansion of $^{14}ND_3$ seeded in krypton via a PZT-actuated pulsed valve. The valve nozzle is constructed from a 2 cm long piece of hypodermic needle tubing and is resistively heated to approximately 185 °C to increase the population of molecules in excited rotational states. The molecular beam, with an initial mean velocity of 460 m/s, passes through a skimmer into a differentially pumped vacuum chamber containing the 149-stage Stark decelerator operating at ±12 kV. After deceleration, the molecules are detected via a $|J,K\rangle$ state sensitive 2 + 1 resonance enhanced multiphoton ionization (REMPI) scheme near 317 nm. The ions are then accelerated by the TOFMS onto the MCP. The signal at the arrival time for an ion with a mass-to-charge ratio of 20 is measured and averaged over many experimental runs.

Operation of the Stark decelerator begins by setting the high-voltage switching timings appropriate for the desired final velocity. This timing sequence is calculated from trajectory simulations using electric fields generated from Comsol, a finite element analysis package. To facilitate the discussion of how these timing sequences are related to different rotational states, we introduce the effective dipole moment,

$$\mu_{eff}=|\vec{\mu}|\frac{MK}{J(J+1)}. \tag{2}$$

For the $|J,K,M\rangle=|1,1,1\rangle,|2,2,2\rangle,$ and $|3,3,3\rangle$ states, $\frac{\mu_{eff}}{\mu}=\frac{1}{2},\frac{2}{3}$, and $\frac{3}{4}$, respectively. Although $\mu_{eff}$ does not uniquely determine the rotational state of the molecule, it does uniquely determine the timing sequence. Therefore, to slow synchronous molecules with different $\mu_{eff}$ values to the same final velocity requires operating the decelerator using different timings. For example, with our particular apparatus, decelerating a $|1,1,1\rangle$ synchronous molecule ($\frac{\mu_{eff}}{\mu}=\frac{1}{2}$, see Table 1) from 460 m/s to 60 m/s requires calculating decelerator timings for a phase angle of $\phi_0\approx 84^\circ$. Removing the same amount of energy per stage for a synchronous molecule with $\frac{\mu_{eff}}{\mu}=5$ requires a much smaller phase angle of $\phi_0\approx 7^\circ$. Calculated switch timings for decelerating the $|2,2,2\rangle$ and $|3,3,3\rangle$ states to 60 m/s, relative to the $|1,1,1\rangle$ state, appear in Fig. 3. Even though the effective dipole moments vary from those of the $|1,1,1\rangle$ state by as much as 50%, the resulting switch timings differ by at most 2.5%. The inset in Fig. 3 contains the relative timings for a hypothetical $ND_3$ molecular state with $\frac{\mu_{eff}}{\mu}=5$.

Note that while the Stark shift depends on $M$, our molecular detection scheme is $M$-independent. Hence, when discussing timings for the decelerator, the full $|J,K,M\rangle$ of the synchronous molecule used to calculate the timings is referenced. Discussion regarding the actual detection of molecules references only $|J,K\rangle$, as all possible values of $M$ are included.

When evaluating the state selectivity of the Stark decelerator we consider only the relative populations in weak-field-seeking states. States that are strong-field-seeking as well as those unperturbed by the electric field will effectively be filtered out. The former are attracted to the highest electric fields, located at the surface of the electrodes, and therefore do not make it to the end of the decelerator. The latter are unguided transversely and not decelerated longitudinally and hence make up a portion of the undecelerated background molecular beam.

To test how the final molecule density depends on the chosen timing sequence, we measure relative populations of decelerated rotational states using timing sequences for synchronous molecules with $\frac{\mu_{eff}}{\mu}=\frac{1}{2},\frac{2}{3},\frac{3}{4},2,3,4,$ and 5 decelerated to 60 m/s. A final velocity of 60 m/s is the lower limit for the $|1,1,1\rangle$ synchronous molecule given our beam's initial forward velocity and our number of decelerator stages. This constitutes a removal of more than 98% of the initial longitudinal kinetic energy of the molecular beam. This velocity was chosen for these measurements because a low final velocity results in decelerated molecules that are spatially displaced from the undecelerated background molecular beam. This displacement effectively amplifies any state selectivity of the decelerator as the undecelerated background molecular beam has a state purity determined solely by the dynamics of the supersonic expansion.

## 5. Results and discussion

The distribution of rotational states initially present in the molecular beam was determined using the setup shown in Fig. 2, but with no voltage applied to the decelerator (free flight). Though not a thermal distribution, the approximate temperature was found to be 6–7 K by fitting the measured spectrum (Fig. 4A) to a theoretical spectrum weighted by Maxwell–Boltzmann factors. The theoretical spectrum was derived from the Hamiltonian for $ND_3$ using constants together with individual line strength calculations from [33,34]. As shown in Fig. 4A, the initial molecular beam consists of numerous excited rotational states. The experimental spectrum has power broadened linewidths of ~0.25 $cm^{-1}$, which is narrow enough that, for our chosen detection wavelengths, adjacent lines do not overlap, thus allowing for true single-state detection. Fig. 4B shows the densities of molecules in states $|1,1\rangle,|2,2\rangle,|2,1\rangle$ and $|3,3\rangle$ as a function of detection time under free flight conditions. The traces have been normalized to the

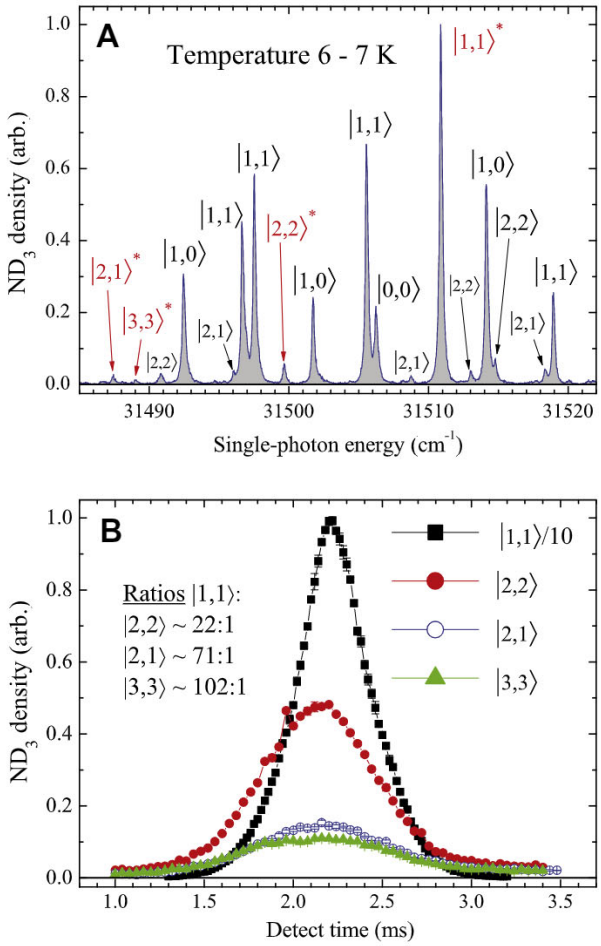


**Fig. 4.** Characterizations of the initial molecular beam. (A) Measured REMPI trace of the molecular beam rotational state distribution where numerous rotational states are populated. The relative state populations indicate an approximate temperature of 6–7 K. (B) Time-of-flight signal of various rotational states at the end of the decelerator where no voltage is applied, as detected on the starred wavelengths in (A). Note that the $|1,1\rangle$ state (solid squares) has been divided by 10 for ease of comparison.

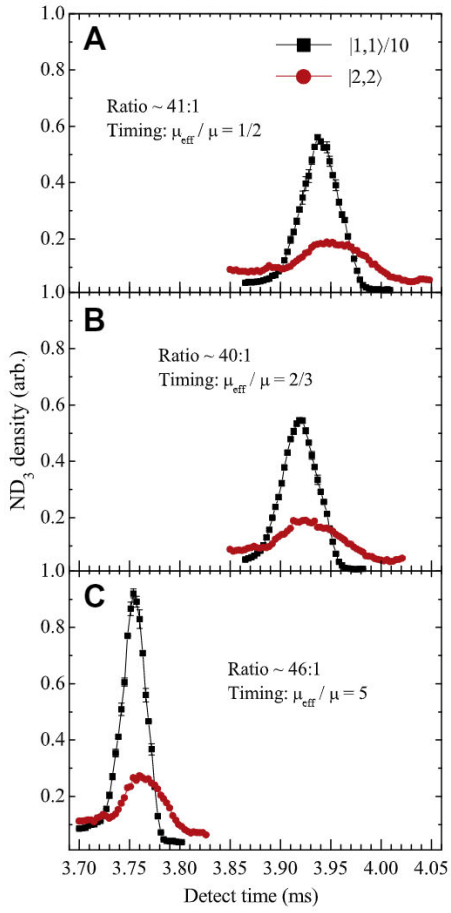


**Fig. 5.** (A) Detecting $|1,1\rangle$ (squares) and $|2,2\rangle$ (circles) molecules with timings calculated for decelerating a $\frac{\mu_{eff}}{\mu}=\frac{1}{2}$ synchronous molecule to 60 m/s. (B) Same as A but using a $\frac{\mu_{eff}}{\mu}=\frac{2}{3}$ timing sequence. (C) Same as A but using an $\frac{\mu_{eff}}{\mu}=5$ timing sequence. Note the comparable ratios and the shift in arrival times.

calculated transition line strengths and are therefore on a common vertical scale to facilitate direct comparison. The $|1,1\rangle$ trace has also been divided by 10 for display purposes. Relative rotational-state populations initially present in the molecular beam are quantified using ratios of peak molecule densities with the initial free-flight ratio of $|1,1\rangle:|2,2\rangle$ being ~22:1.

The ratio of $|1,1\rangle:|2,2\rangle$ is also measured after the deceleration process. If Stark deceleration were capable of generating a molecular beam consisting of a single rotational state, this ratio would exhibit a strong dependence on the timing sequence used. For instance, the ratio would be maximized when using timings calculated with $\frac{\mu_{eff}}{\mu}=\frac{1}{2}$ (i.e. for a $|1,1,1\rangle$ synchronous molecule). Conversely, this ratio should approach zero when using timings determined with $\frac{\mu_{eff}}{\mu}=\frac{2}{3}$ (i.e. for a $|2,2,2\rangle$ synchronous molecule). Observation of no dependence on the timing sequence would indicate no purification of these two states by the Stark deceleration process. Measured time-of-flight molecule densities of the $|1,1\rangle$ and $|2,2\rangle$ states are shown in Fig. 5 for timings calculated using $\frac{\mu_{eff}}{\mu}=\frac{1}{2},\frac{2}{3}$, and 5 synchronous molecules slowed to 60 m/s. The ratio of the density of $|1,1\rangle$ to $|2,2\rangle$ molecules does not change appreciably, even when the timing sequence for a dipole moment an order of magnitude larger is used. Thus, deceleration has little effect on the relative populations of these weak-field-seeking states as no correlation between state purity and timing sequence is observed.

Comparing the ratio of $|1,1\rangle:|2,2\rangle$ between free flight and deceleration using $\frac{\mu_{eff}}{\mu}=\frac{1}{2}$ timing we see an increase of a factor of 2 (from 22:1 to 41:1). The *same* increase in the $|1,1\rangle:|2,2\rangle$ ratio is seen when using $\frac{\mu_{eff}}{\mu}=\frac{2}{3}$ timing (from 22:1 to 40:1), which indicates the effect is not due to the state selectivity of the deceleration process. This increase is primarily due to all $M$ sublevels being present in the free-flight beam, but not in the decelerated beam. Specifically, 1/5 of the $|2,2\rangle$ molecules ($|2,2,2\rangle$ only) are decelerated compared to 1/3 of the $|1,1\rangle$ molecules ($|1,1,1\rangle$ only). The weak-field-seeking $|2,2,1\rangle$ molecules are absent in the decelerated beam because their Stark shift is too small to be decelerated down to these velocities. In addition to the $M$ sub-level contribution, the $|2,2\rangle$ molecules have a 50% wider initial velocity distribution than the $|1,1\rangle$ molecules after the supersonic expansion, decreasing the efficiency of the deceleration process and increasing the ratio of $|1,1\rangle:|2,2\rangle$.

To further explore the effect of various timing sequences on state selectivity, a single state was detected using timing sequences for $\frac{\mu_{eff}}{\mu}=\frac{1}{2},\frac{2}{3},\frac{3}{4},2,3,4,$ and 5 (Fig. 6). Increasing molecular densities are observed when timing sequences for larger $\frac{\mu_{eff}}{\mu}$ are used, regardless of the state being detected. This behavior can be compared to results from a series of three-dimensional Monte Carlo simulations. The simulated density as a function of time-of-flight of $|1,1\rangle$ and $|2,2\rangle$ molecules is shown in Fig. 6B and D, respectively. The simulations correctly predict both the shift in arrival times as well as the increase in molecule density.

The simulations were also used to extract information about the final beam that is difficult to determine experimentally. Of

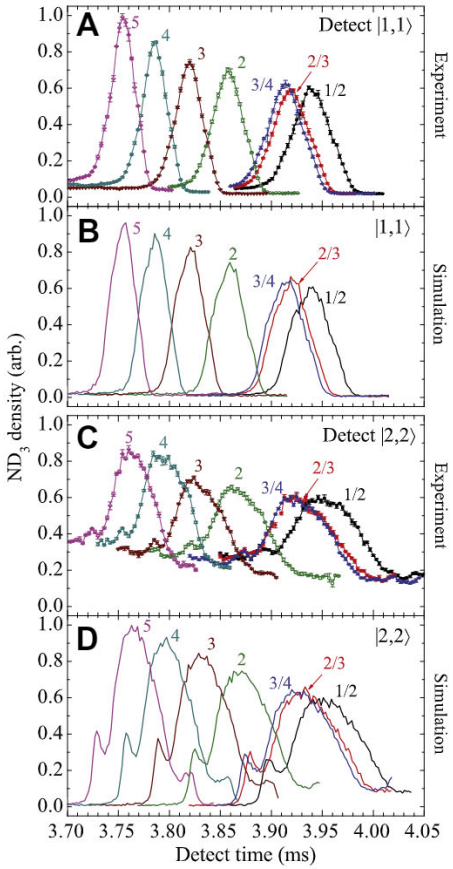


**Fig. 6.** Comparison of experiment and simulation. Time-of-flight traces are labeled by the corresponding $\frac{\mu_{eff}}{\mu}$ value used to calculate the decelerator timing sequence. (A) Detecting $|1,1\rangle$ using various timing sequences calculated using synchronous molecules with different $\mu_{eff}$ values. (B) Results from 3D Monte Carlo simulations of the expected $|1,1\rangle$ densities. (C) Detecting $|2,2\rangle$ under the same conditions as in A. (D) Results from simulations for $|2,2\rangle$.

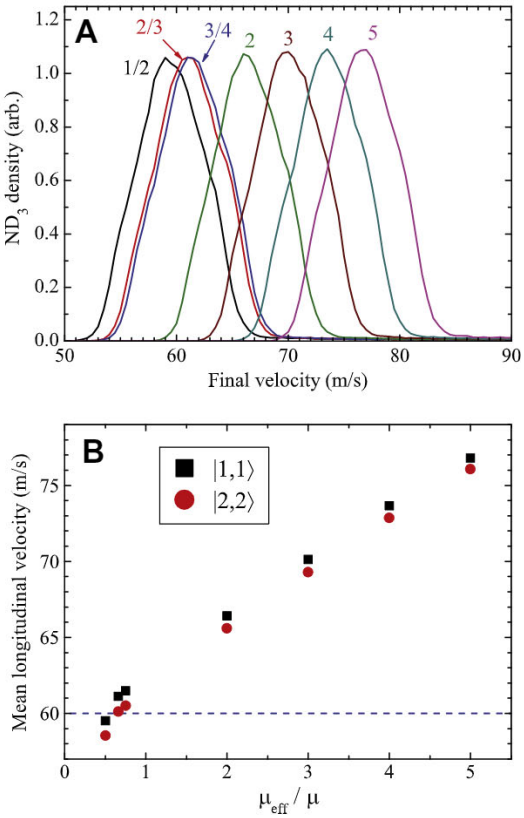


**Fig. 7.** Resulting final velocity distribution for molecules in the $|1,1\rangle$ state using various $\frac{\mu_{eff}}{\mu}$-value timing sequences as produced by Monte Carlo simulations. (A) Curves are labeled by the corresponding $\frac{\mu_{eff}}{\mu}$ value used to calculate the decelerator timing sequence. (B) Mean longitudinal velocities extracted from simulations.

particular interest are the final molecular velocity distributions at the exit of the decelerator under different timing schemes. As shown in Fig. 7, decelerator timing sequences based on larger $\mu_{eff}$ result in increased final velocities. This shift in velocity, together with the timing difference of the last stage (Fig. 3), combine to produce the observed shift in the arrival times (Fig. 6). Fig. 7B shows the final mean longitudinal velocity for both $|1,1\rangle$ molecules and $|2,2\rangle$ molecules. The resulting final velocities for these two states are nearly identical under all timing conditions. In a single realization of the experiment, only one timing sequence can be used, resulting in a molecular beam consisting of both $|1,1\rangle$ and $|2,2\rangle$ molecules with nearly identical final velocities and spatial distributions. Thus both of these states will be present in the resulting decelerated molecular beam.

There are a number of general conclusions to be drawn from these data and simulations. In the case where states with comparable $\mu_{eff}$ values are present, not only will they be decelerated with similar efficiencies, they will exit the decelerator with nearly identical final velocities. Only when the states populating the beam have significantly different Stark shift to mass ratios will they exit the decelerator with substantially different final velocities (Fig. 7). The amount to which the decelerated molecular beam is contaminated with states other than that state desired depends on the population distribution of the initial beam as well as the range of values of $\mu_{eff}$. If a significant fraction of molecules have a $\mu_{eff}$ such that they can be decelerated to the desired final velocity, their contribution to the final beam must be carefully considered.

The state selectivity and resulting beam dynamics of a Stark-decelerated molecular beam have been thoroughly investigated. Our results show that in many circumstances Stark deceleration is not capable of filtering out all but one weak-field-seeking state present in the molecular beam. In fact, every weak-field-seeking state present in the supersonic expansion that can be decelerated to the desired final velocity will be decelerated, regardless of whether its Stark shift is stronger or weaker than that of the synchronous molecule. To improve the state purity of the decelerated beam, other techniques would need to be employed. One option is an electrostatic guide, such as a hexapole, with a Stark-shift dependent focal length. Alternatively, unwanted weak-field-seeking states could be removed by driving them into strong-field seeking states, which will collide with the decelerator electrodes. For ammonia, this could be accomplished using microwaves to transfer the unwanted rotational state(s) into the lower inversion doublet. In any case, producing a molecular beam consisting of just a single quantum state, when the initial beam consists of numerous states amenable to deceleration, requires additional components and introduces new experimental challenges. It is important to note that relative insensitivity of the deceleration process to the Stark shift to mass ratio makes the method very robust to variations in experimental parameters such as the applied electric fields. The state selectivity and velocity distributions of the final decelerated molecular beam is an important consideration when planning and interpreting results of collision experiments using Stark deceleration and analogous techniques.

## Acknowledgments

This work was supported by NSF (PHY 0551010 and PHY 0748742), Air Force Office of Scientific Research (FA9550-08-1-

0193 and FA9550-09-1-0588), and the Alfred P. Sloan Foundation. The authors thank Jun Ye and Ben Stuhl for helpful discussions.

## References

[1] E.R. Hudson, H.J. Lewandowski, B.C. Sawyer, J. Ye, Phys. Rev. Lett. 96 (2006) 143004.
[2] J. Gilijamse, S. Hoekstra, S.Y.T. van de Meerakker, G.C. Groenenboom, G. Meijer, Science 313 (2006) 1617–1620.
[3] L.P. Parazzoli, N.J. Fitch, D.S. Lobser, H.J. Lewandowski, New J. Phys. 11 (2009) 055031.
[4] H.L. Bethlem, G. Berden, A.J.A. van Roij, F.M.H. Crompvoets, G. Meijer, Phys. Rev. Lett. 84 (2000) 5744–5747.
[5] G. Scoles, Atomic and Molecular Beam Methods, 1, Oxford University Press, New York, 1988.
[6] J.D. Weinstein, R. deCarvalho, T. Guillet, B. Friedrich, J.M. Doyle, Nature 395 (1998) 148–150.
[7] D. Patterson, J.M. Doyle, J. Chem. Phys. 126 (2007).
[8] S.A. Rangwala, T. Junglen, T. Rieger, P.W.H. Pinkse, G. Rempe, Phys. Rev. A 67 (2003) 043406.
[9] M.S. Elioff, J.J. Valentini, D.W. Chandler, Science 302 (2003) 1940–1943.
[10] J.M. Sage, S. Sainis, T. Bergeman, D. DeMille, Phys. Rev. Lett. 94 (2005) 203001.
[11] D. Wang, J. Qi, M.F. Stone, O. Nikolayeva, H. Wang, B. Hattaway, S.D. Gensemer, P.L. Gould, E.E. Eyler, W.C. Stwalley, Phys. Rev. Lett. 93 (2004) 243005.
[12] K.-K. Ni, S. Ospelkaus, M.H.G. de Miranda, A. Pe'er, B. Neyenhuis, J.J. Zirbel, S. Kotochigova, P.S. Julienne, D.S. Jin, J. Ye, Science 322 (2008) 231–235.
[13] J.G. Danzl, M.J. Mark, E. Haller, M. Gustavsson, R. Hart, J. Aldegunde, J.M. Hutson, H.C. Nagerl, Laser Phys. 20 (2010) 23–31.
[14] R. Fulton, A.I. Bishop, M.N. Shneider, P.F. Barker, Nat. Phys. 2 (2006) 465–468.
[15] E. Narevicius, A. Libson, C.G. Parthey, I. Chavez, J. Narevicius, U. Even, M.G. Raizen, Phys. Rev. Lett. 100 (2008) 093003.
[16] H.L. Bethlem, G. Berden, G. Meijer, Phys. Rev. Lett. 83 (1999) 1558–1561.
[17] H.K. Bethlem, F.M.H. Crompvoets, R.T. Jongma, S.Y.T. van de Meerakker, G. Meijer, Phys. Rev. A 65 (2002) 053416.
[18] J.R. Bochinski, E.R. Hudson, H.J. Lewandowski, G. Meijer, J. Ye, Phys. Rev. Lett. 91 (2003) 243001.
[19] S.Y.T. van de Meerakker, I. Labazan, S. Hoekstra, J. Kuepper, G. Meijer, J. Phys. B 39 (2006) 1077–1084.
[20] O. Bucicov, M. Nowak, S. Jung, G. Meijer, E. Tiemann, C. Lisdat, Eur. Phys. J.D 46 (2008) 463–469.
[21] T.E. Wall, J.F. Kanem, J.M. Dyne, J.J. Hudson, B.E. Sauer, E.A. Hinds, M.R. Tarbutt, Phys. Chem. Chem. Phys. 13 (2011) 18991–18999.
[22] A.I. Bishop, L. Wang, P.F. Barker, New J. Phys. 12 (2010) 073028.
[23] L.P. Parazzoli, N.J. Fitch, P.S. Zuchowski, J.M. Hutson, H.J. Lewandowski, Phys. Rev. Lett. 106 (2011) 193201.
[24] B.C. Sawyer, B.K. Stuhl, M. Yeo, T.V. Tscherbul, M.T. Hummon, Y. Xia, J. Klos, D. Patterson, J. Doyle, J. Ye, Phys. Chem. Chem. Phys. 13 (2011) 19059.
[25] B.C. Sawyer, B.K. Stuhl, D. Wang, M. Yeo, J. Ye, Phys. Rev. Lett. 101 (2008) 203203.
[26] M. Kirste, L. Scharfenberg, J. Klos, F. Lique, M.H. Alexander, G. Meijer, S.Y.T. van de Meerakker, Phys. Rev. A 82 (2010) 042717.
[27] L. Scharfenberg, J. Klos, P.J. Dagdigian, M.H. Alexander, G. Meijer, S.Y.T. van de Meerakker, Phys. Chem. Chem. Phys. 12 (2010) 10660–10670.
[28] L. Scharfenberg, K.B. Gubbels, M. Kirste, G.C. Groenenboom, A. van der Avoid, G. Meijer, S.Y.T. van de Meerakker, Eur. Phys. J.D 65 (2011) 189–198.
[29] S.Y.T. van de Meerakker, Deceleration and Electrostatic Trapping of OH Radicals, Ph.D. thesis, Radboud Universiteit Nijmegen, 2006.
[30] A. Osterwalder, S.A. Meek, G. Hammer, H. Haak, G. Meijer, Phys. Rev. A 81 (2010) 051401.
[31] S.Y.T. van de Meerakker, N. Vanhaecke, H.L. Bethlem, G. Meijer, Phys. Rev. A 71 (2005) 053409.
[32] P.S. Żuchowski, J.M. Hutson, Phys. Rev. A 79 (2009) 062708.
[33] M.N.R. Ashfold, R.N. Dixon, R.J. Stickland, C.M. Western, Chem. Phys. Lett. 138 (1987) 201–208.
[34] J. Bentley, B.J. Cotterell, A. Langham, R.J. Stickland, Chem. Phys. Lett. 332 (2000) 85–92.